nature chemical biology

ARTICLES

https://doi.org/10.1038/s41589-018-0223-0

Small-molecule allosteric inhibitors of BAX

Thomas P. Garner[1,2,3,4], Dulguun Amgalan[2,3,4,5], Denis E. Reyna[1,2,3,4], Sheng Li[6], Richard N. Kitsis[2,3,4,5] and Evripidis Gavathiotis[1,2,3,4]*

BAX is a critical effector of the mitochondrial cell death pathway in response to a diverse range of stimuli in physiological and disease contexts. Upon binding by BH3-only proteins, cytosolic BAX undergoes conformational activation and translocation, resulting in mitochondrial outer-membrane permeabilization. Efforts to rationally target BAX and develop inhibitors have been elusive, despite the clear therapeutic potential of inhibiting BAX-mediated cell death in a host of diseases. Here, we describe a class of small-molecule BAX inhibitors, termed BAIs, that bind directly to a previously unrecognized pocket and allosterically inhibit BAX activation. BAI binding around the hydrophobic helix α5 using hydrophobic and hydrogen bonding interactions stabilizes key areas of the hydrophobic core. BAIs inhibit conformational events in BAX activation that prevent BAX mitochondrial translocation and oligomerization. Our data highlight a novel paradigm for effective and selective pharmacological targeting of BAX to enable rational development of inhibitors of BAX-mediated cell death.

Programmed cell death is a physiological process in multicellular organisms that clears unhealthy and excess cells to ensure healthy development and tissue homeostasis[1]. In response to acute injury or chronic stress conditions, loss of cells through programmed cell death contributes to the pathogenesis of numerous diseases including myocardial infarction, stroke, toxicity from chemotherapy and radiation and various neurological diseases[2–4]. Genetic and biochemical studies have revealed a crucial role for the BCL-2 family proteins in regulating apoptotic cell death[5,6]. The BCL-2 protein family has anti- and pro-apoptotic members that antagonistically regulate mitochondrial outer-membrane permeabilization (MOMP) and mitochondrial dysfunction[7,8]. Activation of pro-apoptotic BAX and/or BAK by BH3-only proteins is essential for induction of MOMP, whereas anti-apoptotic members inhibit pro-apoptotic members to prevent MOMP[7–9]. MOMP allows the cytoplasmic release of cytochrome *c*, Smac/Diablo and other pro-apoptotic factors from mitochondria, which enables the activation of the apoptotic signaling cascade[10].

Whereas BAK resides constitutively at the MOM, BAX is located predominantly in the cytoplasm, as inactive monomers or dimers and must translocate to the MOM upon activation by BH3-only proteins[11,12] Once activated, BAX and BAK undergo homo- or hetero-oligomerization at the MOM to permeabilize the membrane[13]. Recent studies expanded the function of BAX to regulate necrosis through regulating the opening of the mitochondrial permeability transition pore[14,15]. Interestingly, for this function, translocation, but not oligomerization, of BAX at the MOM is required. Additionally, despite the notion of redundancy for BAX and BAK activity, genetic deletion of BAX alone leads to profound protection from stress-induced cell death in various disease models[16–19]. These studies strongly suggest that BAX may be an attractive target for the pharmacological inhibition of cell death.

Despite significant advances in targeting BCL-2 proteins with small molecules to re-activate cell death in tumors[20,21], efforts to rationally target these proteins to prevent cell death are elusive. Previous attempts led to small molecules that inhibit BAX and BAK channels and oligomerization providing useful insights[22–25]. Lack of structural information for these inhibitors bound to BAX or BAK, however, has impeded their rational development. Moreover, BAX can still promote mitochondrial dysfunction without the requirement for oligomerization, indicating that inhibition at an earlier step of BAX activation would be more effective[14,15].

Here, we focused on the rational inhibition of BAX using recent advances that we have made in studying BAX structure and activation. Previous reports identified sites that regulate BAX activation by the BH3-only proteins, such as the N-terminal trigger site and the canonical groove, which becomes available upon C-terminal helix α9 release (Fig. 1a,b)[26,27]. Additionally, distinct inhibitory binding sites on BAX that interact with peptides from the BH4 domain of BCL-2 and the cytomegalovirus protein vMIA were also identified (Fig. 1c)[28,29]. We recently reported the first rational discovery of small molecules that bind the N-terminal trigger site and activate BAX to promote apoptosis[30,31]. Though we embarked on screening approaches to find inhibitors of BAX, we unexpectedly found select carbazole-based compounds previously reported to inhibit BAX and BAK mitochondrial-associated channels[22,24]. These molecules enabled us to identify a novel binding site on BAX and a new allosteric mechanism of BAX inhibition resulting from binding at this site. Our findings may prove useful for delineating more precisely the mechanistic roles of BAX and provide a rational approach to the development of BAX inhibitors for diseases mediated by BAX-dependent cell death.

Results

Discovery of direct BAX activation inhibitors. To identify direct BAX inhibitors, we have performed screens of small molecules using the liposomal release assay. In this assay, compounds are evaluated for their ability to inhibit membrane permeabilization induced by tBID-mediated BAX activation. Inhibition in this assay can result from impairment of various steps in the BAX activation pathway, including conformational activation, translocation to the liposomal membrane, and oligomerization[25,31,32]. Two carbazole-based compounds were evaluated that differ only with respect to the presence of an –OH or –F group in the piperazinyl-propyl

[1]Department of Biochemistry, Albert Einstein College of Medicine, Bronx, NY, USA. [2]Department of Medicine, Albert Einstein College of Medicine, Bronx, NY, USA. [3]Wilf Family Cardiovascular Research Institute, Albert Einstein College of Medicine, Bronx, NY, USA. [4]Albert Einstein Cancer Center, Albert Einstein College of Medicine, Bronx, NY, USA. [5]Department of Cell Biology, Albert Einstein College of Medicine, Bronx, NY, USA. [6]Department of Medicine, University of California, San Diego, La Jolla, CA, USA. *e-mail: evripidis.gavathiotis@einstein.yu.edu

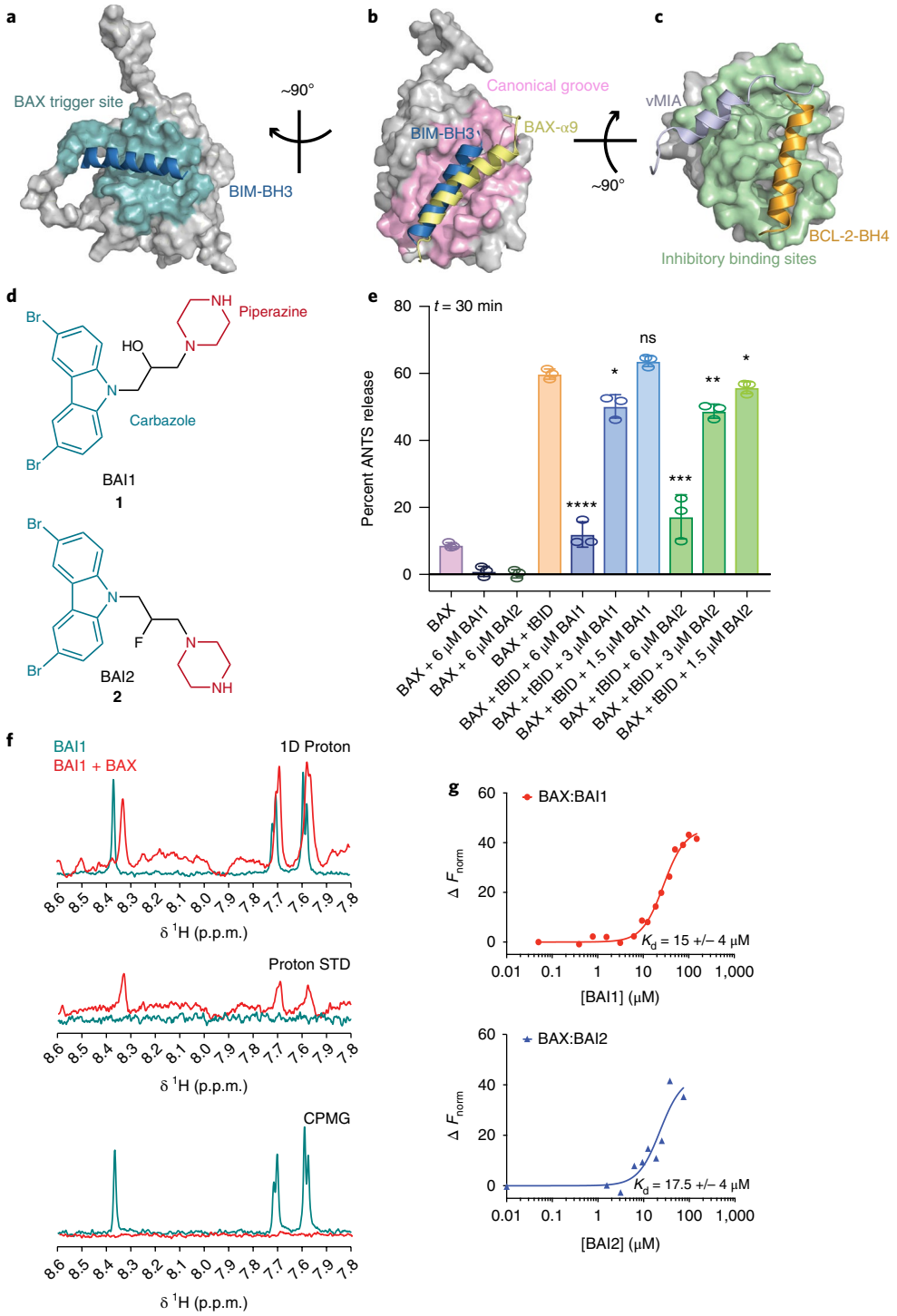

Fig. 1 | BAI1 and BAI2 bind directly to BAX and inhibit BAX activation. a–c, Surface representation of BAX inactive monomer (gray; PDB: 1F16) showing the location of the BAX trigger site (teal) and where BIM BH3 (blue) is bound (**a**), the canonical BH3 groove (pink) where the α9 helix (yellow) and BIM-BH3 (blue) are bound (**b**) and the combined inhibitory binding site (green) where BCL-2 BH4 peptide (orange) and the vMIA peptide (violet) are bound (**c**). **d**, Chemical structures of BAI1 and BAI2. The carbazole (blue) and piperazine (red) ring are labeled for clarity. **e**, BAX-mediated membrane permeabilization assay using liposomes with 400 nM BAX, 1.5–6 μM BAI compounds and 30 nM tBID at $t = 30$ min. Data represent mean ± s.d. of $n = 3$ replicates; data are representative of five independent experiments. Two-sided t-test, **** $P < 0.0001$; ***$P < 0.001$;**$P < 0.01$; *$P < 0.05$; ns, $P > 0.05$. P values were 0.000035, 0.0116, 0.0588, 0.0004, 0.00176, 0.0389, from left to right. **f**, Ligand-observed 1D ^{1}H-NMR of the aromatic peaks of BAI1 (teal) shows chemical shift changes upon addition of inactive BAX (red). A ^{1}H-NMR STD transfer experiment shows the appearance of aromatic peaks of BAI1 in the presence of BAX (red). A ^{1}H-NMR CPMG experiment shows peak broadening of aromatic peaks of BAI1 (teal) in the presence of BAX (red). BAX, 15 μM. BAI1, 150 μM. Data are representative of two independent experiments. **g**, Microscale thermophoretic analysis of the BAX interaction with BAI1 (red) and BAI2 (blue). Single data points are recorded for each titration, and data are representative of two technical replicates and three independent experiments.

extension from the carbazole ring. We named these BAX activation inhibitor 1 (BAI1; **1**) and 2 (BAI2; **2**) (Fig. 1d). BAI1 and BAI2 demonstrated inhibition of tBID-induced BAX-mediated membrane permeabilization in a dose-dependent manner with IC_{50}s of 3.3 μM and 4.6 μM, respectively (Fig. 1e; Supplementary Fig. 1a,b). To confirm direct activity of BAIs on BAX, we compared BAI1's activity in liposome release assays with those of tBID, BIM SAHB and the BAX activator BAM7, as each one has a different affinity for BAX (Supplementary Fig. 1c–e). The observed IC_{50} for BAI1 is independent of both the activating molecule and its concentration, confirming a direct activity on BAX (Supplementary Fig. 1g). In addition, BAI1 was able to inhibit heat-induced BAX activation with a comparable IC_{50} (Supplementary Fig. 1f,g). This prompted us to evaluate direct binding of BAI1 to inactive BAX in solution using ligand-detected ^{1}H-nuclear magnetic resonance (NMR) and microscale thermopheresis (MST) experiments. Upon titration with inactive BAX, proton peaks of the carbazole ring of BAI1 showed evidence of direct and specific binding by either standard 1D ^{1}H, STD and CPMG experiments (Fig. 1f). Moreover, titration of inactive BAX into BAI1 and monitoring of the H3 peak of the carbazole ring by 1D ^{1}H NMR showed dose-dependent chemical-shift perturbation (CSP) and broadening of the peak, consistent with a 1:1 binding ratio (Supplementary Fig. 2). Dissociation constants for BAI1 and BAI2 with BAX of 15.0 ± 4 μM and 17.5 ± 4 μM, respectively, were determined by MST (Fig. 1g; Supplementary Fig. 3). Taken together, these data demonstrate that BAI1 and BAI2 directly bind to BAX.

BAIs bind to inactive BAX at a novel allosteric site. Next, we performed 2D ^{1}H-^{15}N heteronuclear single quantum coherence (HSQC) NMR analysis of ^{15}N-labeled BAX[33]. Addition of BAI1 shifted select NMR cross-peaks while preserving the overall features of the NMR spectra, indicating fast exchange between the bound and unbound conformations of BAX, consistent with a K_d in the low micromolar range (Supplementary Fig. 4). CSP analysis of BAX with BAI1 exhibited significant chemical shifts in residues located at different regions in the protein. The highest changes were observed in select residues of α3, α4, α5 and α6 (Fig. 2a). Although the observed CSPs were smaller than might be expected for an interaction of this nature, they are localized and specific. Interestingly, small CSPs have been observed in previous NMR studies of BAX[26,28–31,34]. To confirm the specificity of these CSPs, we repeated the titration using the analog BAI3, which has ~7-fold lower activity compared to BAI1. We observed significantly reduced CSPs compared to BAI1 (Supplementary Fig. 5). Mapping the BAI1 CSPs onto the structure of inactive BAX revealed that residues undergoing significant shifts are localized at one specific surface of the protein centered where helices α3, α4, α5 and α6 converge (Fig. 2b). Distant from this cluster of residues, a few solvent-exposed residues in helices α1 and α2 and α1–α2 loop also undergo significant CSPs. Interestingly, the region on the surface of BAX, where helices α3, α4, α5 and α6 converge, forms an uncharacterized binding pocket (Fig. 2b).

To support the identification of this pocket, the structure of inactive BAX[33] (PDB ID 1F16) was analyzed with SiteMap (Schrödinger, LLC, 2017), a computational tool to evaluate the propensity of ligand-binding pockets in protein structures. SiteMap suggested five binding pockets for the BAX structure including our newly identified pocket, termed BAI-site, and the BAX trigger site (Supplementary Fig. 6a). By comparing the sites identified by SiteMap with the residues showing significant CSP in our HSQC-NMR titrations, we found that only the BAI-site overlaps with residues undergoing CSP (Supplementary Fig. 6b). Furthermore, we used hy-TEMPO, a soluble paramagnetic relaxation enhancement (PRE) probe, with the idea that such a simple molecule will bind nonspecifically to the solvent-exposed surface, preferentially binding to pockets on the surface of BAX, confirming the presence of the SiteMap-proposed binding pockets[35]. hy-TEMPO induced PRE on the majority of the BAX solvent-exposed residues, with the most significant PREs associated with the BAX trigger site and the BAI-site (Supplementary Fig. 6c–e). This confirmed the presence of a relatively deep solvent-exposed cavity at the proposed interaction site, confirming the existence of the BAI-site on the BAX structure.

We next performed molecular docking of BAI1 using an induced-fit docking approach guided by those residues showing significant CSPs. BAI1 was docked preferentially at the junction of the C terminus of α3, the α3–α4 loop, and the residues of α5 and α6 (Fig. 2c), which is the same region as that suggested by SiteMap (Supplementary Fig. 6e). To account for potential ambiguity in the NMR data, docking was repeated against a largely extended surface of BAX that surrounds the BAI site, yielding only the same docking poses within the BAI site (Supplementary Fig. 7). BAI1 binds consistently with a binding pose that uses the carbazole ring buried near to the hydrophobic core of BAX within the BAI site, whereas the piperazinyl-propanol extension from the carbazole ring is more solvent exposed (Fig. 2d,e). Indeed, this is a reasonable binding mode, as the hydrophobic carbazole ring with the two bromines is surrounded by several aliphatic and aromatic hydrophobic core residues including Val91, Ile136, Leu132, Trp139, Phe116, Val95, Leu185 and Leu120. BAI1 balances these hydrophobic interactions with two potential hydrogen bonds using the piperazinyl-propanol extension (Fig. 2d,e). The positively charged piperazine ring is predicted to form a hydrogen bond with the side chain of Asp84, and the hydroxyl of the propanol is predicted to form a hydrogen bond with the side chain of Lys123 and the main chain carbonyl of Ile80 (Fig. 2d,e). Consistent with this binding mode, Ala81, Lys123 and Val83 cross-peaks undergo the most significant CSP upon titration of BAI1 (Fig. 2a). To further assess the lowest energy docked mode of BAI1, we subjected BAX alone and BAX bound to BAI1 in two independent molecular dynamics (MD) simulations (Supplementary Fig. 8a,b). In both MD simulations, the BAI1 binding mode remained stable within the BAI-site with an average r.m.s. deviation of 0.65 ± 0.31 Å and 0.34 ± 0.1 Å compared to an average r.m.s. deviation of 1.7 ± 0.25 Å and 1.4 ± 0.12 Å for the backbone atoms of the ordered protein regions (Supplementary Fig. 8c,d).

Moreover, we also analyzed BAI2 by HSQC-NMR analysis and docking. The CSP analysis highlighted residues concentrated in the BAI site and a few sporadic CSPs in residues around the BAI site (Supplementary Fig. 9a). Docking of BAI2 is consistent with BAI1 preserving all key interactions (Supplementary Fig. 9b–d). The fluorine atom, however, could not form a hydrogen bond with Ile80 or Lys123, but was able to form a halogen bond with the carbonyl of Ile80.

Lastly, to further confirm the BAI site, we generated two BAX mutants. The first mutant, D84K D86K, was designed to remove hydrogen bonding with the piperizine ring (Fig. 2d,e; Supplementary Fig. 10a)[29]. The second mutant, V83W L120W, was designed to partially fill the proposed binding pocket with tryptophan side chains to potentially mimic BAI binding (Supplementary Fig. 10b,c). Neither BAX mutant showed any effect on retention time in size-exclusion chromatography analysis or the ability of BAX to bind to BIM BH3, suggesting no effect on BAX folding or on the activation site (Supplementary Fig. 11). Both mutants caused significant reduction in the observed CSPs in 2D NMR-based titrations of BAI1, confirming BAI1's interaction with the pocket (Supplementary Fig. 12). Consistently, both mutants resulted in a significant reduction in the inhibition of BAX by BAI1 in response to activation by BH3-only proteins or heat activation at 42 °C (Supplementary Fig. 13a–c). Notably, the V83W L120W mutant showed significant loss in response to BH3-mediated activation in liposome release assays, suggesting a BAI-mimicry inhibition effect as anticipated (Supplementary Fig. 13d,e). Taken together, our results position BAIs at a novel binding site on BAX that is implicated in BAX inhibition.

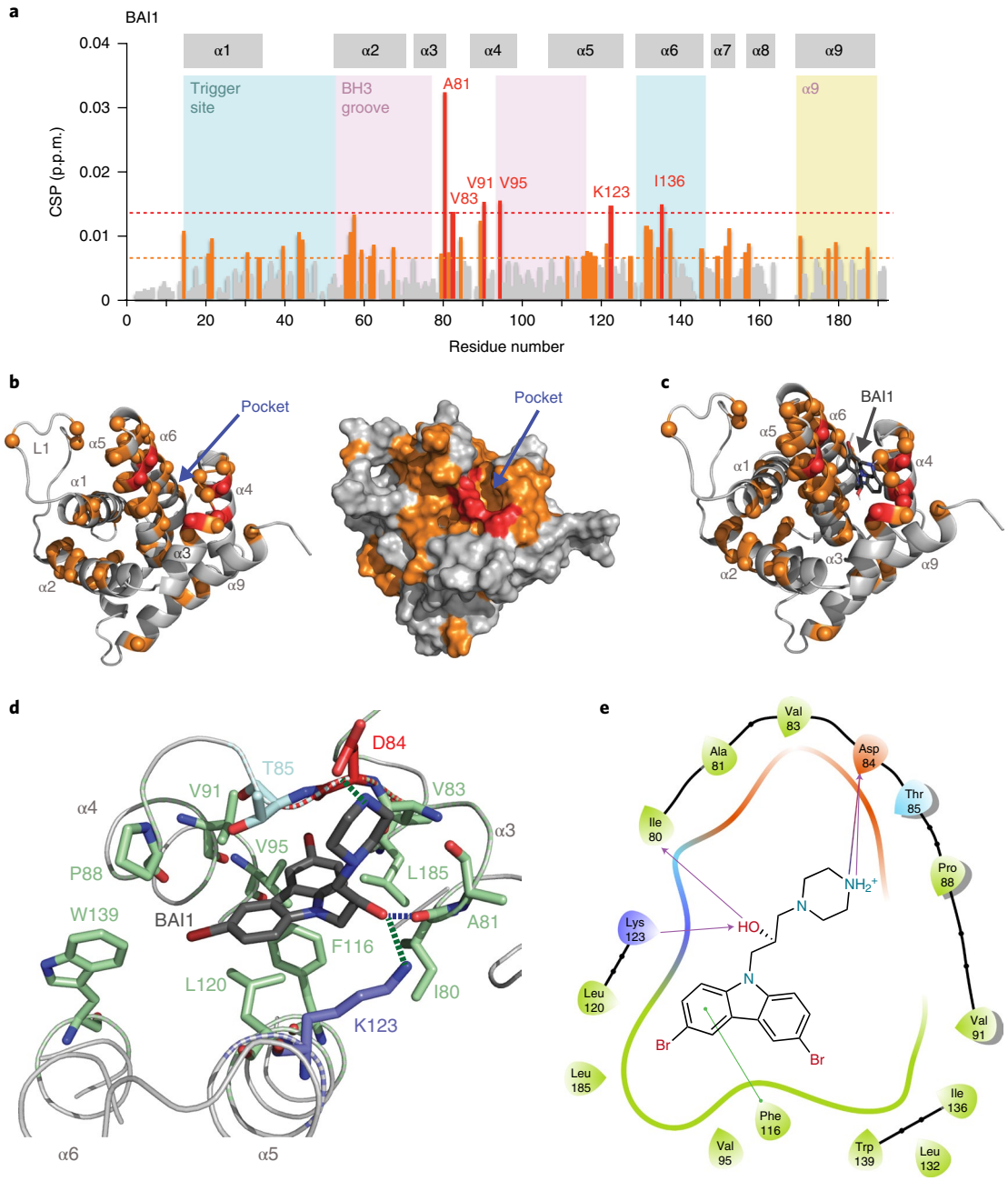

Fig. 2 | BAI1 binds to inactive BAX at a novel allosteric site. a, Measured chemical shift perturbations (CSP) of ^{15}N-labeled BAX upon BAI1 titration up to a ratio of 1:2 BAX:BAI1 are plotted as a function of BAX residue number. Residues with chemical shift ranges over the significance threshold or 1.5 times the threshold are colored orange and red, respectively. Residues associated with the canonical BH3 binding pocket and the BH3 'trigger-site' are indicated with violet and blue shading, respectively; C-terminal helix α9 is shaded yellow. Residues showing CSP > 1.5 times the threshold are labeled for clarity. Data are representative of three independent experiments. **b**, Mapping of residues undergoing significant CSP onto the ribbon and surface representation of BAX (gray; PDB: 1F16), as in **a**, in orange and red color. Residues with significant and the highest CSP concentrate into a grove (blue arrow) that is formed by helices α3, α4 and α5 and loop α3–α4. **c**, Ribbon representation of BAX and mapping of the residues undergoing significant CSP as in **b**. The most energetically favorable docked structure of BAI1 was calculated by the molecular docking software Glide, guided by NMR-based restraints. **d**, Close-up view of the novel binding site and bound docked structure of BAI1 (gray). Favorable hydrophobic contacts, hydrogen bonds and salt bridges between BAI1 BAX are illustrated. **e**, BAX–BAI1 interaction cartoon showing key hydrophobic contacts and hydrogen bonds.

Structure–activity relationships (SAR) of BAIs. Next, we evaluated the contribution of each functional group of the BAI scaffold to the binding and inhibition of BAX. We used ligand-observed CSP calculated by 1D ^{1}H-NMR of the aromatic peaks of BAIs to measure the binding interaction (Supplementary Fig. 14a,b). We also used the liposomal release assay to measure BAX inhibition (Supplementary Fig. 14c). Supplementary Table 1 shows structures of BAI compounds and their corresponding ligand-observed CSP and IC_{50} values in BAX-mediated membrane permeabilization. Loss of each bromine group from the carbazole ring in BAI3 (**3**) and BAI4 (**4**) reduces BAX binding and inhibition, and BAI3 with unsubstituted carbazole has worse binding and inhibition activity. The smaller chlorine group in BAI5 (**5**) compared to the bromine group in BAI4 resulted in less binding, but slightly better BAX

inhibition. The morpholino group in BAI6 (**6**) resulted in reduced inhibition compared to the piperazine group of BAI1, and when the piperazine group is replaced with one or two propyl groups, as in BAI7 (**7**) and BAI8 (**8**), binding and inhibition were reduced. This SAR is likely explained by the morpholino ring possessing no hydrogen bond donor and the one or two propyl groups not aligning for hydrogen bonding as well as the piperazine ring. Interestingly, we found that the carbazole ring can be replaced with the phenothiazine group in BAI9 (**9**) and BAI10 (**10**) with a modest change in activity. This suggests that additional substituted tricyclic or bicyclic ring systems could fit into the BAI-site. Overall, the SAR is consistent with the hydrophobicity and shape complementarity of the di-substituted carbazole-based compounds and potential hydrogen bonding interactions of the piperazine ring. Positive correlation of binding affinity to the BAI-site and inhibition of BAX can inform future rational design strategy for the development of BAX inhibitors (Supplementary Table 1; Supplementary Fig. 14d).

BAIs allosterically inhibit BAX activation in solution. Whereas the C-terminal canonical pocket is buried from its interaction with α9, the BAX trigger site is available for binding in the inactive BAX structure[26,36] (Fig. 1a,b). The BAI site is geographically distinct from the N-terminal trigger site and the C-terminal canonical pocket. Therefore, we hypothesized that BAIs inhibit BAX through a noncompetitive inhibition mechanism. Two other known peptides from BCL-2 and vMIA proteins have been shown to bind and inhibit BAX[28,29] (Fig. 1c). Interestingly, by comparing the structural models of the BCL-2 and vMIA peptides bound to BAX, we found that the vMIA peptide binds at the back surface of the BAI site (Supplementary Fig. 15a). Indeed, some peripheral residues of the BAI site that do not interact with BAI interact with the vMIA peptide (Supplementary Fig. 15a–c)[29]. Although the mechanism of how vMIA peptide inhibits BAX is not fully understood, it has been proposed that it can promote BAX translocation and block BAX oligomerization by binding at this region near the C-terminal helix of BAX[29]. We used the program DYNAFIT (BioKin) to simulate the competition of BAI1 with vMIA and tested this using a fluorescence polarization assay with the vMIA peptide and BAX. We found that addition of BAI1 had no effect on the affinity of the vMIA peptide to BAX, consistent with our structural analysis (Supplementary Fig. 15d). Therefore, the binding site and mechanism of BAI-mediated BAX inhibition appears to be distinct from that of vMIA.

As BAIs bind to inactive BAX, we evaluated how BAI1 affects BH3-mediated BAX activation. BH3 binding to BAX induces conformational changes that transform the inactive soluble monomer into an oligomer[36,37]. Early conformational changes upon BAX activation involve the opening of the α1–α2 loop from the trigger site, the exposure of the α2 (BH3 domain) and the mobilization of α9 from the canonical pocket[36]. Using ^{15}N-^{1}H HSQC-NMR analysis of ^{15}N-labeled full-length BAX, we monitored BAX activation over time upon addition of BIM SAHB (Fig. 3). The addition of BIM SAHB leads to activation of the inactive BAX, as demonstrated by the broadening and reduction of the BAX monomer cross-peaks over time (Fig. 3a,b). Within a few hours, the majority of BAX monomer cross-peaks disappeared below the detection limit (Fig. 3c). Only peaks corresponding to the flexible N terminus of oligomerized BAX can be detected in the activated state. By contrast, in the presence of BAI1, BIM SAHB-induced BAX activation is strongly inhibited with ~80% of the BAX remaining monomeric at 24 h after BIM SAHB addition (Fig. 3d–f). We monitored BAI1 inhibition over an extended time frame and, even after 12 d, 50% of the BAX monomer was present in the NMR sample (Fig. 3f). Next, we calculated CSPs of BAX spectra in the presence of both BIM SAHB and BAI1 (Supplementary Fig. 16a). Significant CSPs were observed in both the BIM SAHB-binding site (trigger site) and the BAI site (Supplementary Fig. 16b,c), suggesting that both BIM SAHB and BAI1 are bound to BAX and that BAI1 effectively blocks the conformational activation of BAX induced by BIM SAHB. BAI1 was not able to fully inhibit BIM SAHB-induced activation of the BAI-site mutants D84K D86K and V83W L120W as monitored by ^{15}N-^{1}H HSQC-NMR analysis, consistent with their loss of binding and activity (Supplementary Fig. 17). To confirm these results with an alternative method, we used size-exclusion chromatography. BIM SAHB induced complete BAX oligomerization of the BAX monomer, whereas BAI1 strongly inhibited the effect of BIM SAHB and preserved BAX as a monomer after 24 h (Supplementary Fig. 18). Taken together, these data demonstrate that BAI1 is a potent inhibitor of BAX conformational activation and oligomerization in solution, not by direct competition with the activator but rather through an allosteric mechanism that favors the inactive BAX.

Mechanism of BAI-induced BAX inhibition. To further interrogate the mechanism of BAI-induced BAX inhibition, we performed hydrogen deuterium exchange mass spectrometry (HXMS) to probe the direct and indirect effects on the protein structure upon BAI1 binding. We calculated the difference in the accessibility of deuterium on inactive BAX unbound and bound to BAI1 (Supplementary Fig. 19a–c). HXMS analysis showed protection in different regions of the BAX structure upon BAI1 binding, which included residues associated with the BAI site (α3-α4, α5) but also pronounced effects in residues of α1, the α1–α2 loop, α3, α7, α8 and α9 associated with the BAX trigger site, as well as regions undergoing conformational changes upon BAX activation (Supplementary Fig. 19c,d). BAI1 increased deuterium incorporation only in residues of α6 and α7. Next, we measured PRE effects using the soluble PRE probe, hy-TEMPO, to account for changes in hy-TEMPO access to the BAX surface in the presence or absence of BAI1. The observed differences in PRE effects demonstrated protection from hy-TEMPO access to the BAX structure induced by BAI1 within the BAI-site (α3–α4, α5), but also in α3, α6, α7, α8 and α9 regions that undergo conformational changes upon BAX activation (Fig. 4a). Only a few isolated residues showed significantly increased access to hy-TEMPO binding due to BAI1 binding (Fig. 4a). Mapping of the PRE effects on the structure of BAX revealed that BAI1 binding leads to significant protection of several regions around the BAI-site and particularly within the hydrophobic core residues of helix α5, which is key to maintaining the inactive BAX structure (Fig. 4b). These local and global effects of BAI1 probed by HXMS and PRE analysis are remarkable for a small molecule and suggest that the inhibitory effect of BAI1 is mediated by direct and allosteric stabilization of key areas of the BAX structure, resulting in suppression of conformational activation.

As BAI1 suppresses conformational changes induced by BH3-only proteins, we investigated biochemical evidence for inhibiting BAX activation, dimerization and MOMP. Indeed, we found that BAI1 inhibited tBID-induced BAX dimers and oligomers formed in the presence of liposomal membranes as detected by BMH cross-linking and SDS–PAGE analysis (Fig. 4c,d). Moreover, BAI1 inhibited BAX membrane association and translocation induced either by tBID ($IC_{50} = 5 \pm 1$ μM) or BIM SAHB ($IC_{50} = 2 \pm 1$ μM) in a dose-dependent manner (Fig. 4e; Supplementary Fig. 20) and with a similar IC_{50} to BAX-mediated liposomal release (Supplementary Table 1). These data are consistent with BAI1 inhibiting the conformational change of the BH3 domain (α2) and the membrane anchoring C-terminal helix α9 required for dimerization and translocation, respectively[27,36]. One of the earliest conformational changes upon BH3-mediated BAX activation is the exposure of the BH3 residues recognized by the anti-BH3 domain antibody[27,36]. In a pull-down assay with anti-BH3 domain antibody, BIM SAHB induced the exposure of the BH3 domain from BAX, and this was suppressed by BAI1 (Fig. 4f,g; Supplementary Fig. 21). Because BAI1 inhibits the early conformational changes seen in BAX activation,

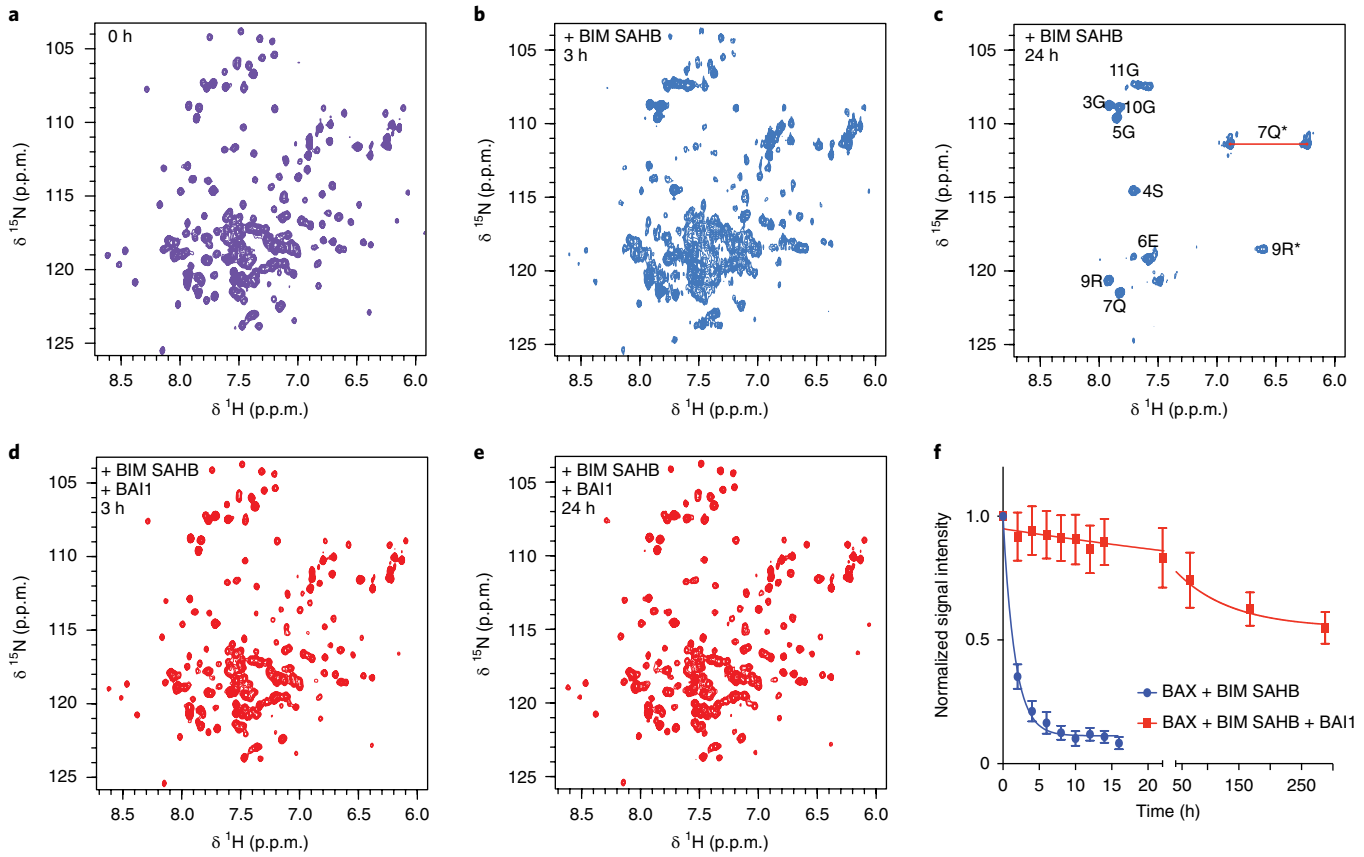

Fig. 3 | BAI1 allosterically inhibits BIM BH3-mediated BAX activation and oligomerization. a–c, ^{15}N-HSQC spectra of ^{15}N-labeled BAX, incubated with BIM SAHB at 0 h (**a**), 3 h (**b**) and 24 h (**c**). BAX activation and oligomerization was monitored by cross-peaks of signal loss of monomeric BAX. **d**,**e**, ^{15}N-HSQC spectra of ^{15}N-labeled BAX, incubated with BIM SAHB, with BAI1, at 3 h (**d**) and 24 h (**e**). **f**, NMR signal intensity of cross-peaks of monomeric BAX over time for BAX incubated without (blue) and with BAI1 (red) after treatment with BIM SAHB. BAX monomer, 50 μM; BAI1, 100 μM; BIM SAHB, 60 μM. Data represent the mean ± s.d. of signal loss of four well resolved NMR peaks, normalized to four peaks with constant NMR intensity throughout the experiment. Data in **a**–**f** are representative of two independent experiments.

we investigated whether BAI1 can stabilize BAX. We measured the temperature-dependent activation of BAX using a translocation assay (Fig. 4h). For BAX alone we measured an activation temperature of ~50 °C, almost 15 °C lower than the reported melting temperature for BAX[38]. The addition of BAI1 caused significant stabilization of BAX with a 10 °C increase in the activation temperature. Taken together, our biochemical and structural data are in agreement with an allosteric mechanism of inhibition of BAX conformational activation by BAI1.

BAI1 selectively inhibits BAX-dependent cell death. Based on the BAI1 inhibition mechanism, we reasoned that BAI1 should selectively inhibit BAX-mediated apoptotic cell death. To test this, we used mouse embryonic fibroblasts (MEF) and promoted apoptosis with TNFα with cyclohexamide stimulus, which induces activation of BAX and BAK. Titration of BAI1 effectively inhibited TNFα with cyclohexamide-mediated apoptosis monitored by caspase 3/7 activation in a dose-dependent manner (IC_{50} = 1.8 μM) (Fig. 5a). To test selectivity for BAX, we compared wild-type MEFs with mutant MEFs lacking *Bax* (BAX knockout (KO); *Bax*$^{-/-}$) or *Bak* (BAK KO; *Bak*$^{-/-}$). Although BAI1 inhibited TNFα + cyclohexamide-mediated-apoptosis in wild-type and BAK KO MEFs (Fig. 5b,c), it had no effect in BAX KO MEFs (Fig. 5d). Next, we evaluated the effect of BAI1 on BAX-induced mitochondrial depolarization mediated by BIM BH3 peptide. Using MEFs deficient for both *Bax* and *Bak* (*Bax*$^{-/-}$; *Bak*$^{-/-}$) that had been reconstituted with human *Bax*, we found that BAI1 dose-dependently inhibited BIM BH3-induced mitochondrial depolarization. (Fig. 5e). Moreover, BAI1 inhibited cell death in OCI-AML3 cells induced by BTSA1, a direct BAX activator through interaction with the trigger site (Fig. 5f). Taken together, these studies demonstrate the selectivity of BAI1 to inhibit BAX activation and BAX-mediated cell death.

Discussion

Our studies highlight small-molecule BAX inhibitors that target a novel binding site on inactive BAX to inhibit BAX activation. This binding site has features ideal for a druggable pocket to facilitate potent and selective targeting of BAX, including a deep hydrophobic groove that is surrounded by polar and charged residues. This pocket is distinct from the already identified binding sites on BAX that interact with BH3-only peptides (to activate BAX) or the inhibitory peptides from the BCL-2 and vMIA proteins[26–29]. Our data are consistent with BAIs operating through a mechanism of inhibition that stabilizes interactions within the hydrophobic core of BAX, thereby inhibiting the induction of conformational changes, including the mobilization of both the BH3 domain and the C-terminal helix α9 from the hydrophobic core, which are critical to BAX dimerization/oligomerization and mitochondrial translocation[5,37]. Binding of BAI1 to BAX does not inhibit the binding of the BH3 activators to the BAX trigger site, but changes the consequences of the binding leading to these conformational changes. The BAI site is distal from both known BH3 activation sites and the sites at which the BH3 domain and α9 are localized on the BAX structure; therefore, we consider the mechanism of BAI1 to be that of an allosteric inhibitor of BAX activation.

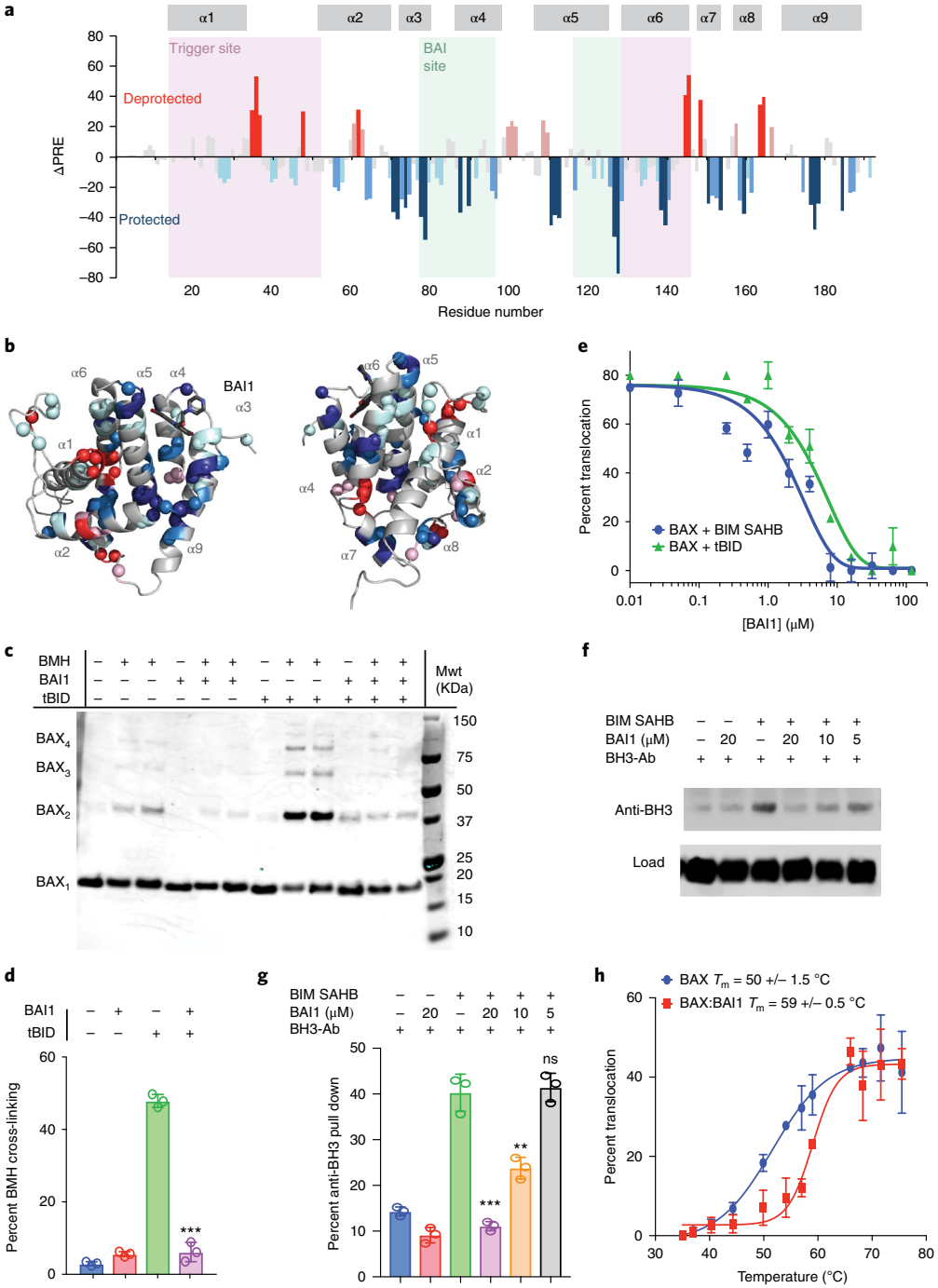

Fig. 4 | Structural and biochemical mechanism of BAI1-mediated BAX inhibition. a, BAI1 induced differences in peak intensity ratio (PRE) of BAX cross-peaks in the presence and absence of the soluble paramagnetic agent hy-TEMPO (Iox/Ired). Residues with PRE differences over the significance threshold of one, two or three times below the negative threshold are colored light blue, blue and dark blue, respectively, and those over one or two times the positive threshold are colored pink and red, respectively. Residues associated with the BAI1 binding pocket and the BH3 'trigger site' are indicated with green and blue shading, respectively. **b**, Ribbon representation of the lowest energy BAX:BAI1 model, with mapping of backbone N atoms of the residues undergoing significant differences in PRE, as shown in **a**, in blue and red color shaded spheres. **c**, BAX membrane oligomerization assay upon tBID-mediated BAX activation in the presence of liposomes with or without BAI1, measured by BMH mediated cross-linking and analyzed by western blot analysis. **d**, Quantification of western blot bands in **c** based on IR fluorescence. Data represent the mean ± s.d. $n = 3$ replicates, and data are representative of two independent experiments. **e**, Quantitative BAX liposomal membrane translocation assay upon tBID-mediated (green) and BIM BH3-mediated (blue) BAX activation in the absence or presence of increasing concentrations of BAI1. Data represent mean ± s.d.; $n = 3$ replicates, and data are representative of five independent experiments. **f**, BIM BH3-mediated BAX activation and immunoprecipitation assay using the anti-BH3 antibody in the absence or presence of increasing concentrations of BAI1. Full blot can be found in Supplementary Fig. 21. **g**, Quantification of western blot bands in **f** based on IR fluorescence. Data represent mean ± s.d.; $n = 3$ replicates, and data are representative of two independent experiments. **h**, Quantitative BAX liposomal membrane translocation assay induced by increasing temperature with and without 6 μM BAI1. The activation temperature (T_m) and error as determined by Prism is annotated for clarity. Data represent mean ± s.d.; $n = 3$ replicates, data are representative of two independent experiments. Two-sided *t*-test, ****$P < 0.0001$, ***$P < 0.001$, **$P < 0.01$, *$P < 0.05$; ns, $P > 0.05$ for BAI1 treated compared to tBID or BIM alone (*P* values were 0.061 for **d** and 0.00047, 0.00469, 0.999 for **g**, from left to right).

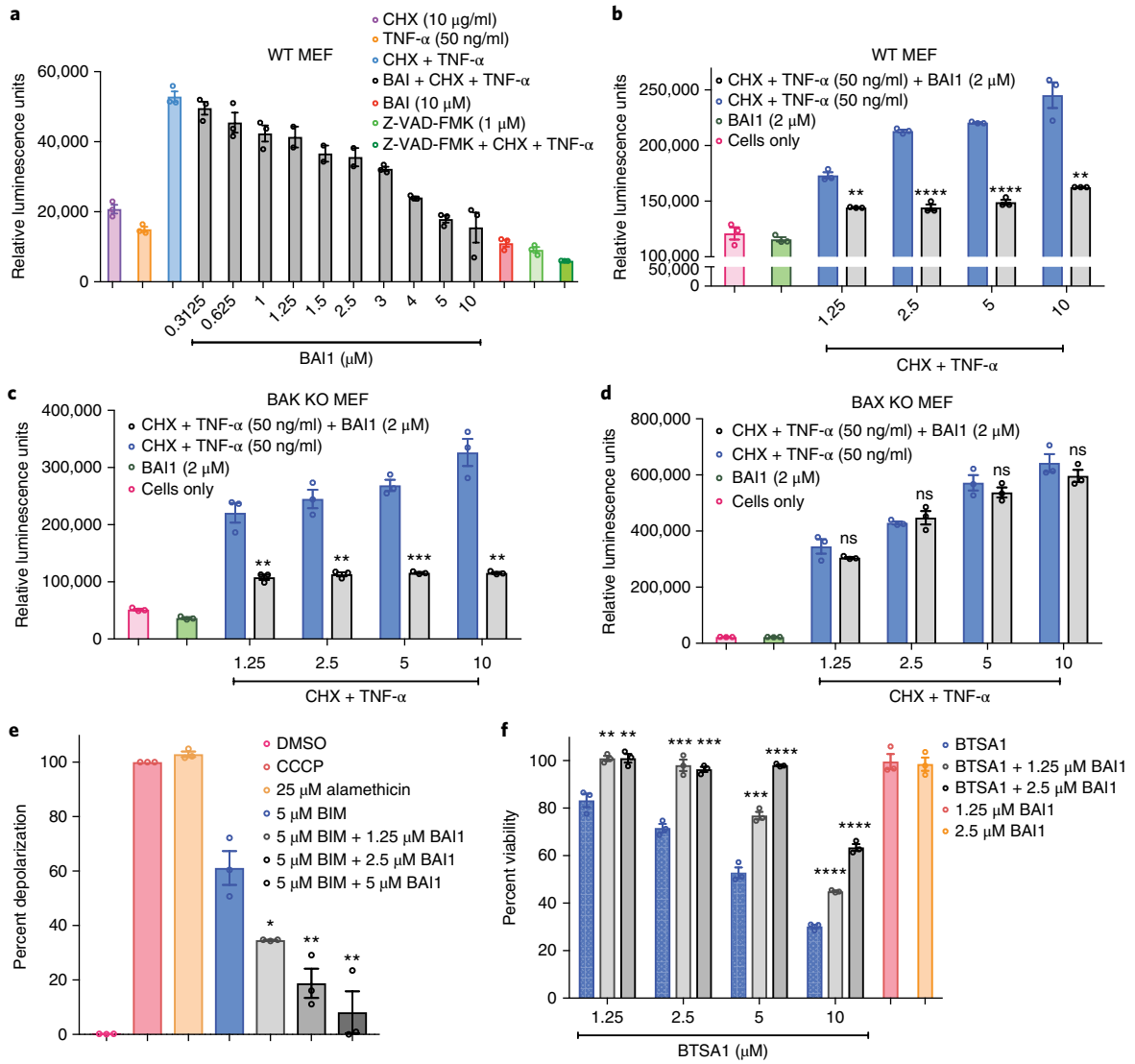

Fig. 5 | BAI1 inhibits cell death in BAX-dependent manner. a, Caspase 3/7 assay of WT MEFs upon pro-apoptotic TNFα and/or CHX treatment in the absence or presence of co-treatment with BAI1 at indicated doses for 8 h. **b**–**d**, Caspase 3/7 assay of WT MEFs (**b**), BAK KO MEFs (**c**) and BAX KO MEFs (**d**) upon pro-apoptotic TNFα/CHX treatment in the absence or presence of co-treatment with BAI1 at 2 μM for 8 h. **e**, Mitochondrial depolarization measured by JC-1 staining of BAX/BAK DKO MEFs reconstituted with human BAX treated with 5 μM BIM BH3 in the absence or presence of BAI1 at indicated doses. Data were collected at 75 min after JC-1 staining. **f**, Viability assay of OCI-AML3 cells upon 6 h treatment with a BAX direct activator BTSA1 in the absence or presence of BAI1 at indicated doses. Data represent mean ± s.d.; $n = 3$ replicates, and data are representative of three independent experiments in all panels. Two-sided *t*-test, $^{****}P < 0.0001$; $^{***}P < 0.001$; $^{**}P < 0.01$, $^{*}P < 0.05$; ns, $P > 0.05$ for BAI1 treatment compared to apoptotic stimulus or BAX activator treatment. *P* values were 0.000538, 0.000023, 0.000006 and 0.0019 for **b**, 0.00315, 0.00134, 0.0001, and 0.00089 for **c**, 0.194, 0.495, 0.351 and 0.292 for **d**, 0.01296, 0.0067 and 0.0058 for **e** and 0.0042, 0.0061, 0.00088, 0.00028, 0.00095, 0.000062 and 0.000036 for **f** from left to right.

BAI1 and BAI2 were first identified from a screen using a BAX-mediated cytochrome *c* release assay as inhibitors of BAX- and BAK-associated channels, and it was suggested that they may promote disassembly of preformed BAX/BAK channels[22,24]. Although inhibition of channel activity by BAI1 and BAI2 is not excluded by our work, the direct effects of these small molecules on BAX had not been evaluated. Nevertheless, our studies suggest that additional carbazole-based compounds, phenothiazine-based compounds and potentially other compounds with fused or unfused ring systems can also bind to the BAI-site of inactive BAX and inhibit BAX activation.

In contrast to BAIs, a fragment from an NMR-based screen was recently shown to bind adjacent to the BAI-site and sensitized BH3-mediated BAX activation[34]. This fragment competed with the binding of the vMIA peptide while allosterically mobilizing the α1–α2 loop and the BAX BH3 domain (α2) adjacent to the trigger site (α1/α6). Such opposite binding effects of this fragment compared to BAIs, despite their adjacent binding location, suggest a remarkable plasticity and allosteric regulation of the BAX structure. Indeed, structural plasticity and allosteric regulation are key properties of the BCL-2 family proteins, which seem critical in the regulation of their mitochondrial localization and protein interactions[26–31,39–44].

In conclusion, we have elucidated a previously unrecognized pocket and an allosteric mechanism of BAX inhibition that can be used by small-molecule BAX inhibitors such as BAIs. BAIs can be used as tools for probing mechanisms of BAX activation and BAX-dependent cell death. Rational targeting of BAX and development of BAX inhibitors through the BAI site offer an

opportunity for therapeutic intervention in disease mediated by BAX-dependent cell death.

Online content

Any methods, additional references, Nature Research reporting summaries, source data, statements of data availability and associated accession codes are available at https://doi.org/10.1038/s41589-018-0223-0.

Received: 29 August 2018; Accepted: 18 December 2018;
Published online: 04 February 2019

References

1. Fuchs, Y. & Steller, H. Programmed cell death in animal development and disease. *Cell* **147**, 742–758 (2011).
2. Whelan, R. S., Kaplinskiy, V. & Kitsis, R. N. Cell death in the pathogenesis of heart disease: mechanisms and significance. *Annu. Rev. Physiol.* **72**, 19–44 (2010).
3. Bredesen, D. E., Rao, R. V. & Mehlen, P. Cell death in the nervous system. *Nature* **443**, 796–802 (2006).
4. Panganiban, R. A., Snow, A. L. & Day, R. M. Mechanisms of radiation toxicity in transformed and non-transformed cells. *Int. J. Mol. Sci.* **14**, 15931–15958 (2013).
5. Youle, R. J. & Strasser, A. The BCL-2 protein family: opposing activities that mediate cell death. *Nat. Rev. Mol. Cell Biol.* **9**, 47–59 (2008).
6. Chipuk, J. E., Moldoveanu, T., Llambi, F., Parsons, M. J. & Green, D. R. The BCL-2 family reunion. *Mol. Cell* **37**, 299–310 (2010).
7. Shamas-Din, A., Kale, J., Leber, B. & Andrews, D. W. Mechanisms of action of Bcl-2 family proteins. *Cold Spring Harb. Perspect. Biol.* **5**, a008714 (2013).
8. Moldoveanu, T., Follis, A. V., Kriwacki, R. W. & Green, D. R. Many players in BCL-2 family affairs. *Trends. Biochem. Sci.* **39**, 101–111 (2014).
9. Luna-Vargas, M. P. & Chipuk, J. E. The deadly landscape of pro-apoptotic BCL-2 proteins in the outer mitochondrial membrane. *FEBS. J.* **283**, 2676–2689 (2016).
10. Tait, S. W. & Green, D. R. Mitochondria and cell death: outer membrane permeabilization and beyond. *Nat. Rev. Mol. Cell Biol.* **11**, 621–632 (2010).
11. Edlich, F. et al. Bcl-x_L retrotranslocates Bax from the mitochondria into the cytosol. *Cell* **145**, 104–116 (2011).
12. Garner, T. P. et al. An autoinhibited dimeric form of BAX regulates the BAX activation pathway. *Mol. Cell* **63**, 485–497 (2016).
13. Dewson, G. & Kluck, R. M. Mechanisms by which bak and bax permeabilise mitochondria during apoptosis. *J. Cell Sci.* **122**, 2801–2808 (2009).
14. Whelan, R. S. et al. Bax regulates primary necrosis through mitochondrial dynamics. *Proc. Natl Acad. Sci. USA* **109**, 6566–6571 (2012).
15. Karch, J. et al. Bax and Bak function as the outer membrane component of the mitochondrial permeability pore in regulating necrotic cell death in mice. *eLife* **2**, e00772 (2013).
16. Perez, G. I. et al. Prolongation of ovarian lifespan into advanced chronological age by Bax-deficiency. *Nat. Genet.* **21**, 200–203 (1999).
17. Libby, R. T. et al. Susceptibility to neurodegeneration in a glaucoma is modified by Bax gene dosage. *PLoS. Genet.* **1**, 17–26 (2005).
18. Ben-Ari, Z. et al. Bax ablation protects against hepatic ischemia/reperfusion injury in transgenic mice. *Liver Transpl.* **13**, 1181–1188 (2007).
19. Hochhauser, E. et al. Bax deficiency reduces infarct size and improves long-term function after myocardial infarction. *Cell Biochem. Biophys.* **47**, 11–20 (2007).
20. Garner, T. P., Lopez, A., Reyna, D. E., Spitz, A. Z. & Gavathiotis, E. Progress in targeting the BCL-2 family of proteins. *Curr. Opin. Chem. Biol.* **39**, 133–142 (2017).
21. Ashkenazi, A., Fairbrother, W. J., Leverson, J. D. & Souers, A. J. From basic apoptosis discoveries to advanced selective BCL-2 family inhibitors. *Nat. Rev. Drug. Discov.* **16**, 273–284 (2017).
22. Bombrun, A. et al. 3,6-Dibromocarbazole piperazine derivatives of 2-propanol as first inhibitors of cytochrome c release via Bax channel modulation. *J. Med. Chem.* **46**, 4365–4368 (2003).
23. Hetz, C. et al. Bax channel inhibitors prevent mitochondrion-mediated apoptosis and protect neurons in a model of global brain ischemia. *J. Biol. Chem.* **280**, 42960–42970 (2005).
24. Peixoto, P. M., Ryu, S. Y., Bombrun, A., Antonsson, B. & Kinnally, K. W. MAC inhibitors suppress mitochondrial apoptosis. *Biochem. J.* **423**, 381–387 (2009).
25. Niu, X. et al. A small-molecule inhibitor of Bax and Bak oligomerization prevents genotoxic cell death and promotes neuroprotection. *Cell Chem. Biol.* **24**, 493–506.e5 (2017).
26. Gavathiotis, E. et al. BAX activation is initiated at a novel interaction site. *Nature* **455**, 1076–1081 (2008).
27. Czabotar, P. E. et al. Bax crystal structures reveal how BH3 domains activate Bax and nucleate its oligomerization to induce apoptosis. *Cell* **152**, 519–531 (2013).
28. Barclay, L. A. et al. Inhibition of pro-apoptotic BAX by a noncanonical interaction mechanism. *Mol. Cell* **57**, 873–886 (2015).
29. Ma, J. et al. Structural mechanism of Bax inhibition by cytomegalovirus protein vMIA. *Proc. Natl Acad. Sci. USA* **109**, 20901–20906 (2012).
30. Gavathiotis, E., Reyna, D. E., Bellairs, J. A., Leshchiner, E. S. & Walensky, L. D. Direct and selective small-molecule activation of proapoptotic BAX. *Nat. Chem. Biol.* **8**, 639–645 (2012).
31. Reyna, D. E. et al. Direct activation of BAX by BTSA1 overcomes apoptosis resistance in acute myeloid leukemia. *Cancer Cell* **32**, 490–505.e10 (2017).
32. Yethon, J. A., Epand, R. F., Leber, B., Epand, R. M. & Andrews, D. W. Interaction with a membrane surface triggers a reversible conformational change in Bax normally associated with induction of apoptosis. *J. Biol. Chem.* **278**, 48935–48941 (2003).
33. Suzuki, M., Youle, R. J. & Tjandra, N. Structure of Bax: coregulation of dimer formation and intracellular localization. *Cell* **103**, 645–654 (2000).
34. Pritz, J. R. et al. Allosteric sensitization of proapoptotic BAX. *Nat. Chem. Biol.* **13**, 961–967 (2017).
35. Deschamps, M. L., Pilka, E. S., Potts, J. R., Campbell, I. D. & Boyd, J. Probing protein-peptide binding surfaces using charged stable free radicals and transverse paramagnetic relaxation enhancement (PRE). *J. Biomol. NMR* **31**, 155–160 (2005).
36. Gavathiotis, E., Reyna, D. E., Davis, M. L., Bird, G. H. & Walensky, L. D. BH3-triggered structural reorganization drives the activation of proapoptotic BAX. *Mol. Cell* **40**, 481–492 (2010).
37. Kim, H. et al. Stepwise activation of BAX and BAK by tBID, BIM, and PUMA initiates mitochondrial apoptosis. *Mol. Cell* **36**, 487–499 (2009).
38. Zhao, G. et al. Activation of the proapoptotic Bcl-2 protein Bax by a small molecule induces tumor cell apoptosis. *Mol. Cell Biol.* **34**, 1198–1207 (2014).
39. Uchime, O. et al. Synthetic antibodies inhibit Bcl-2-associated X protein (BAX) through blockade of the N-terminal activation site. *J. Biol. Chem.* **291**, 89–102 (2016).
40. Leshchiner, E. S., Braun, C. R., Bird, G. H. & Walensky, L. D. Direct activation of full-length proapoptotic BAK. *Proc. Natl Acad. Sci. USA* **110**, E986–E995 (2013).
41. Iyer, S. et al. Identification of an activation site in Bak and mitochondrial Bax triggered by antibodies. *Nat. Commun.* **7**, 11734 (2016).
42. Follis, A. V. et al. Regulation of apoptosis by an intrinsically disordered region of Bcl-xL. *Nat. Chem. Biol.* **14**, 458–465 (2018).
43. Follis, A. V. et al. PUMA binding induces partial unfolding within BCL-xL to disrupt p53 binding and promote apoptosis. *Nat. Chem. Biol.* **9**, 163–168 (2013).
44. Lee, S. et al. Allosteric inhibition of antiapoptotic MCL-1. *Nat. Struct. Mol. Biol.* **23**, 600–607 (2016).

Acknowledgements

We thank B. Agianian and A. Haimowitz for assistance with MST controls and BAX C62S/C126S/S3C mutant preparation. Studies were supported by an American Heart Association Collaborative Science Award (15CSA26240000) to E.G. and R.N.K. Support was also provided by NIH award 1R01CA178394 to E.G. and the Fondation Leducq Transatlantic Network of Excellence grant (RA15CVD04) to E.G. and R.N.K. E.G. is supported by the Pershing Square Sohn Cancer Research Alliance and the Irma T. Hirschl Trust Career Award. NMR data were collected with support from NIH awards 1S10OD016305, P30 CA013330 a grant from NYSTAR.

Author contributions

T.P.G. performed NMR, biochemical and molecular modeling studies. D.E.R. performed cell-based studies, and S.L. performed mass spectrometry studies. D.A. and R.N.K. performed cell-based studies. E.G. conceived the study, designed experiments and wrote the manuscript, which was edited by all authors.

Competing interests

E.G., R.N.K., T.P.G, and D.A. are inventors on a patent application PCT/US2018/021644 submitted by Albert Einstein College of Medicine that covers compounds, compositions and methods for BAX inhibition for the treatment of diseases and disorders.

Additional information

Supplementary information is available for this paper at https://doi.org/10.1038/s41589-018-0223-0.

Reprints and permissions information is available at www.nature.com/reprints.

Correspondence and requests for materials should be addressed to E.G.

Publisher's note: Springer Nature remains neutral with regard to jurisdictional claims in published maps and institutional affiliations.

Methods

Reagents. Hydrocarbon-stapled peptides corresponding to the BH3 domain of BIM, BIM SAHB$_{A2}$: N-acetylated- and FITC-Ahx-EIWIAQELRS5IGDS5FNAYYA-CONH2, where S5 represents the non-natural amino acid inserted for olefin metathesis, were synthesized, purified at > 95% purity by CPC Scientific Inc. and characterized as previously described[30]. vMIA peptide FITC-Ahx-CEALKKALRRHRFLWQRRQRA peptide were synthesized and purified at > 95% purity by Genescript[29]. Recombinant tBID in > 95% purity by SDS–PAGE under reducing conditions was purchased by R&D Systems. BAI1 and related compounds were purchased from Millipore, Sigma and Chembridge, and their molecular identity and purity > 95% was confirmed by NMR and MS analysis. BAM7 was purchased from Selleck and purity > 95% was confirmed by NMR and MS analysis. Compounds were > 95% pure, reconstituted in 100% DMSO and diluted in aqueous buffers or cell culture medium for assays.

Production of recombinant BAX. Human full-length (1–192) wild-type BAX was cloned in pTYB1 vector (New England BioLabs) between the NdeI and SapI restriction sites. Mutations were generated using the QuickChange Lightning site directed mutagenesis kit (Agilent). Recombinant proteins were expressed in BL21 (DE3) CodonPlus (DE3)-RIPL, grown in Luria Broth media and induced with 1 mM isopropyl β-D-1-thiogalactopyranoside. The bacterial pellet was resuspended in lysis buffer (20 mM Tris–HCl pH 7.6, 250 mM NaCl, 1 mM EDTA, and Roche complete EDTA free protease inhibitor cocktail), lysed by high pressure homogenization, and clarified by ultracentrifugation at 45,000 × *g* for 45 min. The supernatant was applied to 5 ml of pre-equilibrated chitin beads (New England BioLabs) in a gravity-flow column, and washed with 3 column volumes of lysis buffer. BAX was cleaved by overnight incubation using 50 mM DTT in lysis buffer. Cleaved BAX was eluted with lysis buffer, concentrated with a Centricon spin concentrator (Millipore) and purified by gel filtration using a using a Superdex 75 10/300 GL, column (GE Healthcare Life Sciences), pre-equilibrated with gel filtration buffer (20 mM HEPES, 150 mM KCl, pH 7.2) at 4 °C. Fractions containing BAX monomer are pooled and concentrated using a 10-KDa cut-off Centricon spin concentrator (Millipore) for prompt use in biochemical and structural studies.

Microscale thermophoresis. Recombinant BAX protein was labeled at cysteine using the Monolith Protein Labeling Kit Red Maleimide (NanoTemper Technologies) according to the instructions of the manufacturer. Briefly, proteins at concentrations of 10 μM were incubated with 1 or 2 equivalents of dye in MST buffer (100 mM potassium phosphate, pH 7.4, 150 mM NaCl) in the dark at room temperature (22–25 °C) for 1 h. Unreacted dye was quenched using 5 mM DTT and removed by filtration through 10 KDa cut-off centrifugal concentrator. Degree of labeling was confirmed after purification by comparing the measured concentration of BAX and bound dye using the OD_{280} and OD_{650}, respectively. To determine the K_d values of BAX to BAI1 and BAI2, 100 nM of labeled BAX was incubated with increasing concentrations of BAIs (150–0.5 μM) for 10 min in MST buffer. Samples were sonicated in a sonicating water bath for 10 s, loaded into standard glass capillaries (Monolith NT.115 Capillaries), and analyzed by MST using a Monolith NT.115 Blue/Red, LED power of 30% and an IR laser power of 40% and 60%. The initial 10-s sonication was used to ensure solubility of the BAI1 at the higher concentrations. Insoluble particles within the capillaries of MST experiments can disrupt diffusion and lead to unusable data points. Binding data was analyzed using GraphPad Prism (GraphPad Software) to determine the K_d values of BAX to BAIs using a 1:1 binding model. For these analyses, the temperature jump (1.6 s) region of the MST curves was used. Labeling of one or both cysteines of BAX, or moving the site of labeling using the mutant C62S C126S S5C, reported essentially the same K_d.

NMR samples and spectroscopy. The uniformly ^{15}N-labeled protein samples were prepared by growing the bacteria in minimal medium as previously described[39]. Unlabeled and ^{15}N-labeled protein samples were prepared in 50 mM potassium phosphate, 50 mM NaCl solution at pH 6.0 in 10% D_2O. All experiments were performed using an independent sample for each experimental measurement as a 55 μl sample in a 1.7-mm microtube; all samples were DMSO matched. We have tested the pH of our NMR sample with and without BAI1 up to 200 μM and found no change in pH (measured pH values of 6.023 ± 0.02 vs. 6.028 ± 0.02, respectively; $n = 8$). Ligand detected NMR experiments were performed using 100–150 μM BAI with and without unlabeled BAX at 10–15 μM, prepared in 50 mM potassium phosphate, 50 mM NaCl solution at pH 6.0 in 10% D_2O. 1D ^{1}H-NMR spectra were recorded using standard methodologies incorporating water suppression using excitation sculpting[45]. STD experiments were performed using an off resonance frequency of −2,000 Hz and an on resonance frequency of 450 Hz employing a saturation time of 0.5–2 s using standard bruker pulse sequence[46]. 1D Carr–Purcell–Meiboom–Gill (CPMG) experiments were performed using standard Bruker pulse sequence employing a relaxation delay of 200 ms[47]. Correlation ^{1}H-^{15}N-HSQC spectra were recorded on ^{15}N-labeled BAX at 50 μM, and titrations up to 150 μM of BAI compounds were performed. NMR spectra were acquired at 25 °C on a Bruker 600 MHz spectrometer equipped with a cryoprobe, processed using TopSpin and analyzed with CCPNMR. BAX cross-peak assignments were applied as previously reported[26] and deposited in BMRB entry 18340 (ref. [33]).

The weighted average chemical shift difference Δ(CSP) was calculated as $\sqrt{(\Delta\delta H1)2 + (\Delta\delta N15/5)2}$ in p.p.m. The absence of a bar indicates no chemical shift difference, the presence of a proline or a residue that is overlapped or missing and therefore not used in the analysis. The significance threshold for backbone amide chemical shift changes (0.01 p.p.m.) was calculated based on the average chemical shift across all residues plus the s.d., in accordance with standard methods[48]. Solvent-accessible surface area was probed by the addition of 10 mM hy-TEMPO (Sigma) to 50 μM ^{15}N-labeled BAX with and without 200 μM BAI1 measured using standard ^{1}H-^{15}N-HSQC incorporating an increased recycle delay of 5 s[35]. PRE was calculated as the ratio of peak intensities of BAX in the presence of hy-TEMPO to BAX without hy-TEMPO (I_{para}/I_{dia}). Mapping of chemical shifts and PRE data onto the BAX structure was performed with PyMOL (Schrodinger, LLC). Software was made available through the SBGrid collaborative network[49].

NMR-based docking calculations and molecular dynamics. Small-molecule binding sites on the BAX structure (PDB ID 1F16) were identified using the program SiteMap (Schrödinger, LLC, 2017)[50]. NMR-guided docking of BAI1 and BAI2 into the NMR structure of BAX (PDB ID 1F16) was performed using GLIDE (Glide, Schrödinger, LLC, 2016) with or without constraints based on residues undergoing significant chemical shifts. BAIs were converted to 3D all atom structure using LIGPREP (Schrödinger, LLC, 2016) and assigned partial charges with EPIK (Schrödinger, LLC, 2016). BAIs were docked using the induced fit docking mode with extra precision (XP) rescoring. To account for potential ambiguity in the NMR data, docking was repeated using a largely extended surface of BAX to include regions surrounding the proposed BAI site including the vMIA peptide, but no new poses were generated. The lowest energy docking pose is consistent with the observed NMR chemical shift perturbation data. The lowest energy structure pose from XP docking was selected for further analysis and subjected to a 50 ns molecular dynamics (MD) simulation using DESMOND (DESMOND, version 3, Schrödinger, LLC, 2017). The lowest energy BAX structure from the NMR ensemble (PDB ID 1F16) was subjected to a 50ns MD simulation using DESMOND for comparison. MD runs were performed in truncated octahedron SPC water box using OPLS_2005 force field, 300K and constant pressure of 1.0325bar. Clustering and analysis of the trajectory was performed with MAESTRO tools (Schrödinger, LLC, 2018). PyMOL (Schrödinger, LLC, 2018) was used for preparing the highlighted poses.

NMR-based BAX activation assay. BAX activation and oligomerization were monitored by ^{1}H-^{15}N-HSQC spectra using BAX at 50 μM and BIM SAHB$_{A2}$ at 60 μM without or with 100 μM BAI1 in the presence of NMR buffer plus 0.25% CHAPS to stabilize the oligomeric BAX in solution and Complete EDTA free Protease inhibitor and 0.05% NaN_3 to prevent degradation. Activation was measured by the time-dependent signal loss upon addition of BIM SAHB$_{A2}$. For this analysis, a selection of well-resolved residues with high starting intensities from the core domain of the protein (L25, A42, E44, and L120) were monitored and normalized to a selection of residues from the flexible N terminus of the protein (G3, S4 and G10), which show little to no signal loss during the experiment. Normalized signal loss was plotted in Prism and fit to a single exponential function. Mutations were assessed as above using a single time-point experiment with 50 μM BAX D84K D86K or V83W L120W, preincubated with 100 μM BAI1 and treated with 60 μM BIM-SAHB$_{A2}$ for 24 h.

BAX oligomerization by gel filtration analysis. Solution oligomerization was analyzed by size-exclusion by incubating 50 μM BAX with 60 μM BIM-SAHB$_{A2}$ with and without 100 μM BAI1 in 50 mM potassium phosphate, 150 mM NaCl solution at pH 6.0 0.25% CHAPS, for 12 h at room temperature. oligomerization reactions were analyzed using a superdex75 gel filtration column ran in the incubation buffer.

Hydrogen-deuterium exchange mass spectrometry. Prior to hydrogen-deuterium exchange experiments, the quench condition for best sequence coverage of BAX was optimized as previously described[12,51]. Briefly, 3 μl of stock solution of BAX at 1.0 mg/ml was mixed with 9 μl of H_2O buffer (8.3 mM Tris, 150 mM NaCl, in H_2O, pH7.2) at 0 °C and then quenched with 18 μl of ice-cold quench solutions of 0.8% formic acid, 16% glycerol, and GdnHCl at final concentrations of 0.05 M, 0.5 M, 1.0 M and 2.0 M. The quenched samples were frozen on dry ice and then subjected to an immobilized pepsin column (1 × 20 mm, 30 mg/ml porcine pepsin (Sigma)) for online digestion for 40 s. The resulting peptides were collected on a C18 trap (Michrom, MAGIC C18AQ 0.2 × 2 mm) and separated using a reversed phase C18 column (Michrom, MAGIC C18AQ 0.2 × 50 mm, 3 μm, 200 Å) with a 30 min linear gradient of 0.046% (v/v) trifluoroacetic acid, 6.4% (v/v) acetonitrile to 0.03% (v/v) trifluoroacetic acid and 38.4% (v/v) acetonitrile. The effluent was directed into an OrbiTtrap Elite mass spectrometer (Thermo Fisher Scientific Inc.) for MS analysis. The instrument was operated in positive ESI mode, and the resolution of the instrument was set at 60,000. Proteome Discoverer software (Thermo Fisher Scientific Inc.) was used to identify the sequence of the resulting peptides. The optimal quench condition with the best coverage map of BAX (0.08 M GndHCl in 0.8% formic acid) was used for subsequent functionally deuterated studies. Hydrogen-deuterium exchange reactions were initiated by diluting 3 μl of

prechilled protein stock solution (BAX monomer, 1 mg/ml, or BAX monomer with BAI1, 2 mg/ml) into 9 µl D_2O buffer (8.3 mM Tris, 150 mM NaCl, in D_2O, pDREAD 7.2). The samples were incubated at 0 °C for 10 s, 100 s and 1,000 s. The exchange reaction was terminated by the addition of 18 µl of optimized quench solution at 0 °C, and samples were immediately frozen on dry ice and stored at −80 °C. In addition, undeuterated samples and equilibrium-deuterated control samples were also prepared as previously described. The deuterated samples were then loaded onto the above described instrument for HXMS analysis. The centroids of the isotopic envelopes of undeuterated, functionally deuterated, and equilibrium deuterated peptides were measured using HDExaminer, and then converted to corresponding deuteration levels with corrections for back-exchange.

Fluorescence polarization binding assays. Fluorescence polarization assays (FPA) were performed as previously described[31]. Direct binding isotherms of vMIA were measured by incubating FITC-vMIA (50 nM) with serial dilutions of full-length BAX in the presence and absence of 100 µM BAI1. Direct binding isotherms of BIM were measured by incubating FITC-BIM-$SAHB_{A2}$ (25 nM) with serial dilutions of full-length BAX, either wild type or with mutations. Fluorescence polarization was measured for 60 min at 10 min intervals on a F200 PRO microplate reader (TECAN). K_d values were calculated by nonlinear regression analysis of all binding curves using Graphpad Prism software fit to a 1:1 binding model. Competitive binding curves for vMIA with BAI1 were simulated using the program DYNAFIT (BioKin) to simulate the competition of BAI1 with vMIA for binding to BAX using a K_d of 15 µM and 140 nM, respectively[52].

Liposomal permeabilization assay. Lipids (Avanti Polar Lipids) at the indicated ratio–phosphatidylcholine 48%, phosphatidylinositol 10%, dioleoyl phosphatidylserine 10%, phosphatidylethanolamine, 28%, and tetraoleoyl cardiolipin 4%—were mixed in total of 4 mg, dried and resuspended in 0.2 mM EDTA, 10 mM HEPES, pH 7, 200 mM KCl, and 5 mM $MgCl_2$ buffer with 12.5 mM 8-aminonaphthalene-1,3,6-trisulfonic acid (ANTS) dye and 45 mM p-xylene-bis-pyridinium bromide (DPX) quencher (Molecular Probes) using a water bath sonicator. Liposomes were formed by extrusion of the suspension using polycarbonate membranes of 0.2 µm pore size (Avanti Polar Lipids). ANTS/DPX encapsulated liposomes were purified from non-encapsulated ANT/DPX by gel filtration over a 10-ml CL2B-Sepharose (GE Healthcare Life Sciences) gravity flow column. BAX (400 nM) was pre-incubated with the indicated concentration of BAI1 in a 96-well format (Corning) at room temperature for 30 min before being mixed with liposomes (10 µl from 50 mM total lipid stock) in assay buffer (10 mM HEPES, pH 7, 200 mM KCl, 1 mM $MgCl_2$) to a final volume of 90 µl. Reactions are initiated by the addition of the indicated activator at the indicated concentrations to make a final volume of 100 µl. ANTS/DPX release was quantified based on the increase in fluorescence intensity that occurs when the ANTS fluorophore is separated from the DPX quencher upon release from the liposomes into the supernatant. Fluorescence (λex = 355 nm and λem = 520 nm) was measured over time at 30 °C using a Tecan Infinite M1000 plate reader. In the case of heat activation, reactions were set up as normal without activating peptide and the experiments recorded at 42 °C for 60–90 min. The percentage release of ANTS/DPX at any given time point was calculated as percentage release = $((F - F_0)/(F_{100} - F_0))$ Å~100, where F_0 and F_{100} are baseline and maximal fluorescence, respectively. 1% Triton treatment is used to determine the maximum amount of liposomal release per assay, and this value sets the 100% value.

BAX oligomerization assay. BAX oligomerization was detected using a cross-linking approach by incubating liposomes and recombinant BAX protein (400 nM) and tBID (60 nM) with and without BAI1 for 25 min at 30 °C followed by incubation with 10× bis-maleimidohexane (BMH, Pierce) for 10–30 min on ice followed by quenching with 1 mM DTT for 10 min. Samples were denatured at 95 °C with 1× LDS loading dye (Invitrogen) and analyzed by 4–12% NuPage (Invitrogen) gel electrophoresis followed by immunoblotting with anti-BAX yth-2d2 antibody (R&D systems).

Western blotting and protein quantification. BAX samples were electrophoretically separated on 4–12% NuPage (Invitrogen) gels, transferred to mobilon-FL PVDF membranes (Millipore) and subjected to immunoblotting. For visualization of proteins with Odyssey Infrared Imaging System (LI-COR Biosciences), membranes were blocked in PBS containing 2.5% milk powder. Primary BAX yth-2d2 antibody (R&D systems, cat. # 2282-MC-100) was incubated overnight at 4 °C in a 1:1,000 dilution. After washing, membranes were incubated with an IRdye800-conjugated goat anti-mouse IgG secondary antibody (LI-COR Biosciences, cat. # 926-68022) in a 1:5,000 dilution. Protein was detected with Odyssey Infrared Imaging System. Densitometry of protein bands were acquired using a LI-COR Odyssey scanner. Quantification and analysis was performed using the Western Analysis tool from the Image Studio 3.1 software.

BAX conformational change assay using the anti-BH3 antibody. Exposure of the BH3 domain of BAX was assessed by immunoprecipitation with a BAX BH3-Domain-specific antibody purchased from Abgent (cat. #AP1302a). Recombinant full-length BAX (200 nM) was incubated with BIM-$SAHB_{A2}$ (800 nM) with and without BAI1 in the presence of liposomes, in assay buffer (10 mM HEPES, 200 mM KCl, 5 mM $MgCl_2$, pH 7.2) for 30 min. After incubation, 1 µl of BAX BH3-domain antibody was added to every sample, mixed with pre-washed protein A/G beads (Santa Cruz) and incubated for 1 h at 4 °C with rotation. Beads were collected by brief spin, washed three times with 1 ml of assay buffer, and then solubilized with 25 µl LDS/DTT loading buffer. Samples were resolved by SDS–PAGE electrophoresis and western blot analysis an anti-BAX yth-2D2 antibody (Invitrogen).

Liposomal translocation assay. Liposomes of the following lipid composition (Avanti Polar Lipids)—phosphatidylcholine, 47%; phosphatidylethanolamine, 27%; phosphatidylinositol, 10%; dioleoyl phosphatidylserine, 10%; tetraoleoyl cardiolipin, 4%; and biotin-phosphatidylethanolamine, 2%—were mixed (1 mg total) and resuspended in liposome assay buffer (10 mM HEPES, 200 mM KCl, 0.2 mM EDTA, 5 mM MgCl2, pH 7.2). The resulting slurry was vortexed for 10 min and sonicated in a sonicating water bath at 4 °C for 10 min. The solution was then passed through an Avanti Mini-Extruder Set (#610000) equipped with a 100-nm filter, followed by passage through a CL2B Sepharose column (GE Healthcare). For the liposomal translocation assay, recombinant BAX (400 nM) is pre-incubated with varying concentrations of BAI1 with the indicated activator at the indicated concentration, in liposome assay buffer in a 96-well low binding plate (Costar) for 3 min at room temperature before the addition of 10 µl of liposome preparation to a total volume of 100 µl. Reaction mixtures were incubated for 45 min at room temperature with shaking. Streptavidin was immobilized onto 96-well EIA/RIA plates (Corning Inc.) at 5 µg per well (incubated at 4 °C over night in PBS) and blocked for 2 h at room temperature with 3% BSA in PBS. Liposome translocation mixtures were mixed with BSA (final concentration 0.6%) immediately before loading on to streptavidin coated 96-well EIA/RIA plate, and incubated for 15 min at room temperature, after which 50 µg of biotin was added to each reaction and incubated for 5 min. Nontranslocated BAX was removed by four washes with PBS. BAX translocation was measured using either horseradish peroxidase (HRP)-N20-anti-BAX or HRP-2D2-anti-BAX antibody conjugate (Santa Cruz sc-493 HRP or sc-20067 HRP), incubated at 1/2,500 dilution in 3% BSA for 1 h at room temperature and washed 4 times with PBS, followed by incubation with 3,3,5,5 -tetramethylbenzidine HRP substrate, quenched with 0.5 M sulfuric acid and measured at 450 nm. Each well was normalized to 100% BAX translocation induced by BAX incubated with 1% triton X and liposomes.

Translocation assay by size-exclusion chromatography. Purified BAX at 1 µM was incubated with liposomes in the presence or absence of 0.2 µM tBID with and without 6 µM BAI1 for 45 min at 30 °C. Membrane associated BAX was separated from soluble BAX by size exclusion chromatography using a 3 ml CL-2B gravity-flow gel filtration column. In total 12 fractions of 250 µl were collected and the presence of BAX detected by western blot analysis. Fractions corresponding to liposomes were determined from control samples containing ANTS/DPX loaded liposomes and were detected by fluorescence.

Activation temperature measurement. Liposomal translocation assay reactions were prepared as described above with the absence of activating peptide. Reaction mixtures were heated on a PCR heat block using a temperature gradient of 35–90 °C for 60–90 min. Liposomes translocation mixtures were incubated with streptavidin plates and analyzed as described above. The temperature dependent activation was used to determine the activation temperature (T_m) by fitting the response using Graphpad Prism software, fit to a Boltzmann sigmoid.

Caspase-3/7 activation and cell viability assays. WT MEFs, BAK KO MEFs and BAX KO MEFs were maintained in DMEM (Life Technologies) supplemented with 10% FBS, 100 U ml−1 penicillin/streptomycin, 2 mM l-glutamine, 0.1 mM MEM nonessential amino acids, and 50 µM β-mercaptoethanol. MEFs (1×10^4 cells/well) were seeded in 96-well opaque plates for 18–24 h and then incubated with TNF + CHX without and with BAI1 or Z-VAD-FMK in DMEM at 37 °C in a final volume of 100 µl. Caspase-3/7 activation was measured at 8 h by addition of the Caspase-Glo 3/7 chemiluminescence reagent in accordance with the manufacturer's protocol (Promega). Luminescence was detected by a F200 PRO microplate reader (TECAN). Caspase assays were performed in at least triplicate. Viability assays with the BAX activator, BTSA1, were performed in OCI-AML3 cells (2.5×10^3 cells/well) seeded in 384-well white plates and incubated with indicated concentrations of BTSA1 and BAI1 or DMSO in no FBS media for 2.5 h, followed by 10% FBS replacement to a final volume of 25 µl. Dilutions of compounds were performed using a TECAN D300e Digital Dispenser from 10 mM stocks. Cell viability was assayed at 6 h by addition of CellTiter-Glo according to the manufacturer's protocol (Promega), and luminescence measured using a F200 PRO microplate reader (TECAN). Viability assays were performed in at least triplicate and the data normalized to vehicle-treated control wells. IC_{50} values were determined by nonlinear regression analysis using Prism software (Graphpad).

Mitochondrial depolarization assay. $BAX^{-/-}/BAK^{-/-}$ MEF reconstituted with human wild type BAX were plated overnight (5,000 cells/well) in a 384-well opaque plate. After 18 h, the media was removed and 50 µL of fresh media was added. Cell

were treated with BAI1 (5 µM, 2.5 µM, 1.25 µM) or DMSO for 2 h; compounds were dispensed using a TECAN D300 digital dispenser. After 2 h, media was removed and cells were washed three times with 1× PBS. Following last wash, 1× PBS was removed from every well and 50 µl of staining solution was added directly into the plate. The staining solution contains a final concentration of 0.02 mg/ml oligomycin, 0.05 mg/ml digitonin, 2 µM JC-1, 0.01 M 2-mercaptoethanol dissolved in MEB solution. The MEB solution contains: 150 mM mannitol, 10 mM HEPES-KOH, 50 mM KCl, 0.02 mM EGTA, 0.02 mM EDTA, 0.1% BSA, 5 mM succinate, pH 7.5. After addition of staining solution, BIM BH3 peptide, CCCP, alamethicin and DMSO were added using TECAN D300 digital dispenser. Fluorescence was measured at 545 nm excitation and 590 nm emission using the M1000 microplate reader (TECAN) at 30°. Percentage of depolarization was calculated by normalization to the solvent-only control (0% depolarization) and the positive control CCCP (100% depolarization). Mitochondrial polarization analysis was performed in triplicates.

Reporting Summary. Further information on experimental design is available in the Nature Research Reporting Summary linked to this article.

Data availability

Data generated or analyzed during the study and included in this published article are available from the corresponding author on reasonable request.

References

45. Hwang, R. L. & Shaka, A. J. Water suppression that works. Excitation sculpting using arbitrary wave-forms and pulsed-field gradients. *J. Magn. Reson.* **A 112**, 275–279 (1995).
46. Mayer, M. & Meyer, B. Characterization of ligand binding by saturation transfer difference NMR spectroscopy. *Angew. Chem. Int. Edn Engl.* **38**, 1784–1788 (1999).
47. Hajduk, P. J., Meadows, R. P. & Fesik, S. W. Discovering high-affinity ligands for proteins. *Science* **278**, 497–499 (1997).
48. Marintchev, A., Frueh, D. & Wagner, G. NMR methods for studying protein-protein interactions involved in translation initiation. *Methods Enzymol.* **430**, 283–331 (2007).
49. Morin, A. et al. Collaboration gets the most out of software. *eLife* **2**, e01456 (2013).
50. Halgren, T. A. Identifying and characterizing binding sites and assessing druggability. *J. Chem. Inf. Model.* **49**, 377–389 (2009).
51. Marsh, J. J. et al. Structural insights into fibrinogen dynamics using amide hydrogen/deuterium exchange mass spectrometry. *Biochemistry* **52**, 5491–5502 (2013).
52. Kuzmic, P. Program DYNAFIT for the analysis of enzyme kinetic data: application to HIV proteinase. *Anal. Biochem.* **237**, 260–273 (1996).